Quantum analysis and experimental investigation of the nondegenerate optical parametric oscillator with unequally injected signal and idler

Ning Wang and Yongmin Li*

State Key Laboratory of Quantum Optics and Quantum Optics Devices, Institute of Opto-Electronics, Shanxi University, Taiyuan 030006, China

(Received 4 December 2014; revised manuscript received 11 November 2015; published 15 January 2016)

We developed a quantum analysis of the nondegenerate optical parametric oscillator (NOPO) with unequally injected signal and idler. Both the steady-state output field and the two-mode quantum correlation spectrum are investigated under the condition of different injected idler-to-signal ratios (ISRs) and the relative phase between the pump and the injected seed. It is found that when the seed is injected through the output coupler, the NOPO allows for the robust generation of two-mode quantum entanglement even if the relative phase is free running and the ISR is as high as 0.7. At the specific relative phase of zero, a high degree of entanglement can exist across a whole range of ISRs. An experimental study of the NOPO with unequal seeds is presented, and the observed results verify the theoretical predictions.

DOI: 10.1103/PhysRevA.93.013831

I. INTRODUCTION

Entanglement is now widely employed as an important resource for quantum information processing, such as quantum communication [1], quantum computing [2], and quantum metrology [3], etc. For instance, it is found that in continuous-variable (CV) quantum key distribution, an entangled-state-based protocol can tolerate much more excess noise of the quantum channel than the coherent-state protocol [4], or equivalently, can have longer secure communication distances and higher secure bit rates. In one-way quantum computation, a highly entangled state, the so-called cluster state is a necessary computational resource [5]. The sensitivity and resolution of phase measurement in a Mach-Zehnder interferometer can reach the sub-Heisenberg sensitivity with the aid of two-mode squeezed vacuum and parity detection [6].

Intracavity second-order nonlinear processes are powerful approaches for the preparation of CV quantum entanglement [7–21]. Among them, the nondegenerate optical parameter oscillator (NOPO) has attracted considerable attention. Actually, the Einstein-Podolsky-Rosen (EPR) paradox was first demonstrated for continuous variables by employing a NOPO below the threshold [7–9]. By injecting both the signal and the idler fields with equal average intensity into the NOPO, bright two-mode squeezed light which has the EPR correlation between the signal and the idler can be generated [10]. When only the signal is injected, quantum entanglement with a relatively intense field has been predicted [22] and experimentally demonstrated [20]. In this scenario, the NOPO operates essentially in a phase-insensitive regime, and the entanglement generation is robust against the relative phase between the pump and the injected signal fields.

Below-threshold NOPO with bright injected fields can generate bright quantum entanglement. The injected seed facilitates the cavity-length stability and the relative phase locking between the local oscillator and the output signal fields in homodyne detection which is necessary to characterize the field quadratures in phase space. Furthermore, wide frequency tunability is also attainable with bright fields. Previous works mainly focused on injecting the NOPO with both the signal and the idler fields where they have the same average intensity or injecting the NOPO with only the signal field where the idler field is absent or equivalent in a vacuum state. Here the quantum properties of the NOPO in a more general case where the injected signal and idler have unequal amplitudes are investaged.

In real experimental conditions, it is difficult to obtain a pure injected signal field when the signal field is derived from the down-conversion field. It is probable that some residual idler field will be mixed in the injected signal field. Such a residual idler field can come from the nonideal filtering of the idler field, the backscattering light from the nonlinear crystal, and the cavity mirror of the NOPO, etc. It is necessary to investigate the effect of such a residual idler field on the quantum entanglement characteristics of the NOPO, i.e., the evolution of the two-mode quantum correlation spectrum versus the different injected idler-to-signal ratios (ISRs) and relative phase between the pump and the injected seed.

In this paper, we present the quantum analysis and experimental investigation of the NOPO for the case of unequally injected signal and idler fields. In Sec. II, we introduce the theoretical model. The steady-state mean-value solutions are derived in Sec. III. Then, a perturbation expansion approach is utilized to deduce linear quantum fluctuation equations for the combined field quadratures in Sec. IV. In Sec. V, based on the results of quantum noise spectrum of the combined field quadratures, we analyze in detail the quantum characteristics of the NOPO under the conditions of different injected signal-to-idler ratios and the relative phases between the pump and the injected seed. In Sec. VI, we present an experimental study of the NOPO with unequal seeds and compare the observed results with the theoretical predictions.

II. THEORETICAL MODEL

The system we study consists of three interacting field modes within a nonlinear resonator, i.e., pump, signal, and idler modes with angular frequencies of ω_0, ω_1, and ω_2, respectively, where the energy conservation relation is satisfied

*Corresponding author: yongmin@sxu.edu.cn

$\omega_0 = \omega_1 + \omega_2$. We assume that the pump field ε_0 is strong and the signal and idler fields are much weaker than the pump with injected fields ε_1 and ε_2, respectively. The intracavity fields at frequencies ω_j ($j = 0-2$) are described by the boson annihilation operators $\hat{a}_j$. $\hat{\Gamma}_j$ denote the reservoir operators which describe the damping of the cavity. χ represents the nonlinear coupling constant of the nonlinear crystal.

The Heisenberg-picture Hamiltonian which describes this model is given by [23]

$$\begin{aligned}
\hat{H} &= \sum_{j=0}^{3} \hat{H}_j, \\
\hat{H}_0 &= \sum_{j=0}^{2} (\hbar\omega_j \hat{a}_j^\dagger \hat{a}_j), \\
\hat{H}_1 &= \sum_{j=0}^{2} i\hbar(\varepsilon_j e^{-i\omega_j t}\hat{a}_j^\dagger - \varepsilon_j^* e^{i\omega_j t}\hat{a}_j), \\
\hat{H}_2 &= i\hbar\chi(\hat{a}_1^\dagger \hat{a}_2^\dagger \hat{a}_0 - \hat{a}_1 \hat{a}_2 \hat{a}_0^\dagger), \\
\hat{H}_3 &= \sum_{j=0}^{2} (\hat{a}_j \hat{\Gamma}_j^\dagger + \hat{a}_j^\dagger \hat{\Gamma}_j).
\end{aligned} \tag{1}$$

In a driven system, the density matrix should be calculated as the solution of a master equation. The master equation for the reduced density operator in a rotating frame, obtained after the elimination of the reservoirs using standard techniques, is given by

$$\frac{\partial\hat{\rho}}{\partial t} = [\hat{H}_0+\hat{H}_1+\hat{H}_2,\hat{\rho}]/i\hbar + \sum_{j=0}^{2} \gamma_j([\hat{a}_j\hat{\rho},\hat{a}_j^\dagger] + [\hat{a}_j,\hat{\rho}\hat{a}_j^\dagger]), \tag{2}$$

where γ_j describe the cavity mode damping rate which is related to the cavity linewidth.

It is convenient to transform Eq. (2) into a Fokker-Planck equation using the positive-P representation [24],

$$\hat{\rho} = \int \frac{|\alpha\rangle\langle(\alpha^+)^*|}{\langle(\alpha^+)^*||\alpha\rangle} P_+(\alpha,\alpha^+) d^6\alpha \; d^6\alpha^+, \tag{3}$$

where $\{\alpha\} \equiv (\alpha_0,\alpha_1,\alpha_2)$ and $\{\alpha^+\} \equiv (\alpha_0^+,\alpha_1^+,\alpha_2^+)$ are two independent triplets of complex variables and $P(\alpha,\alpha^+)$ is a positive phase-space distribution function. By using the above equation and assuming that boundary terms vanish on partial integration, $P(\alpha,\alpha^+)$ satisfies the following Fokker-Planck equation:

$$\begin{aligned}
\frac{\partial P_+}{\partial t} =& \left\{ \frac{\partial}{\partial\alpha_0}[\gamma_0\alpha_0 + \chi\alpha_1\alpha_2 - \varepsilon_0] + \frac{\partial}{\partial\alpha_0^+}[\gamma_0\alpha_0^+ + \chi\alpha_1^+\alpha_2^+ - \varepsilon_0^*] + \frac{\partial}{\partial\alpha_1}[\gamma_1\alpha_1 - \chi\alpha_0\alpha_2^+ - \varepsilon_1] \right. \\
&+ \frac{\partial}{\partial\alpha_1^+}[\gamma_1\alpha_1^+ - \chi\alpha_0^+\alpha_2 - \varepsilon_1^*] + \frac{\partial}{\partial\alpha_2}[\gamma_2\alpha_2 - \chi\alpha_0\alpha_1^+ - \varepsilon_2] + \frac{\partial}{\partial\alpha_2^+}[\gamma_2\alpha_2^+ - \chi\alpha_0^+\alpha_1 - \varepsilon_2^*] \\
&\left. + \frac{\partial^2}{(\partial\alpha_1\partial\alpha_2)}(\chi\alpha_0) + \frac{\partial^2}{(\partial\alpha_1^+\partial\alpha_2^+)}(\chi\alpha_0^+) \right\} P_+(\alpha,\alpha^+,t).
\end{aligned} \tag{4}$$

Equation (4) can be written as the following set of Itô stochastic equations [22]:

$$\begin{aligned}
d\alpha_0 &= (\varepsilon_0 - \gamma_0\alpha_0 - \chi\alpha_1\alpha_2)dt, \quad d\alpha_0^+ = (\varepsilon_0^* - \gamma_0\alpha_0^+ - \chi\alpha_1^+\alpha_2^+)dt, \\
d\alpha_1 &= (\varepsilon_0 - \gamma_1\alpha_1 + \chi\alpha_2^+\alpha_0)dt + \sqrt{\chi\alpha_0}dW_1, \quad d\alpha_1^+ = (\varepsilon_1^* - \gamma_1\alpha_1^+ + \chi\alpha_2\alpha_0^+)dt + \sqrt{\chi\alpha_0^+}dW_1^+, \\
d\alpha_2 &= (\varepsilon_2 - \gamma_2\alpha_2 + \chi\alpha_1^+\alpha_0)dt + \sqrt{\chi\alpha_0}dW_2, \quad d\alpha_2^+ = (\varepsilon_2^* - \gamma_2\alpha_2^+ + \chi\alpha_1\alpha_0^+)dt + \sqrt{\chi\alpha_0^+}dW_2^+,
\end{aligned} \tag{5}$$

where the complex Gaussian noise terms obey the following relations:

$$\langle dW_1\rangle = \langle dW_2\rangle = 0, \quad \langle dW_1 dW_2\rangle = \langle dW_1^+ dW_2^+\rangle = dt. \tag{6}$$

Without loss of generality, we consider the input pump as a real field with $\varepsilon_0 = \varepsilon_0^* = E_0$, the injected signal and idler have the forms of $\varepsilon_1 = E_1 e^{i\varphi_1}$ and $\varepsilon_2 = E_2 e^{i\varphi_2}$, where φ_1 and φ_2 denote the relative phase shift. The field quadratures are defined as

$$X_i' = (\alpha_i + \alpha_i^+), \quad Y_i' = (\alpha_i - \alpha_i^+)/i. \tag{7}$$

For simplicity we set $\gamma_1 = \gamma_2 = \gamma$, $\gamma_r = \gamma_0/\gamma$ and introduce two scaling parameters,

$$g = \chi/(\gamma\sqrt{2\gamma_r}), \quad \tau = \gamma t, \tag{8}$$

and the scaled quadratures,

$$x_0' = g\sqrt{2\gamma_r}X_0', \quad y_0' = g\sqrt{2\gamma_r}Y_0', \quad x_1' = gX_1', \quad y_1' = gY_1', \quad x_2' = gX_2', \quad y_2' = gY_2'. \tag{9}$$

The stochastic equations for the scaled quadratures are

$$\begin{aligned}
dx_0' &= -\gamma_r[x_0' - 2\mu_0 + (x_1'x_2' - y_1'y_2')]d\tau, \\
dy_0' &= -\gamma_r[y_0' + (x_1'y_2' + x_2'y_1')]d\tau, \\
dx_1' &= [-x_1' + 2\mu_1\cos(\varphi_1) + (x_0'x_2' + y_0'y_2')/2]d\tau + g(\sqrt{x_0' + iy_0'}dw_1 + \sqrt{x_0' - iy_0'}dw_1^+)/\sqrt{2},
\end{aligned}$$

$$dy_1' = [-y_1' + 2\mu_1 \sin(\varphi_1) + (y_0'x_2' - x_0'y_2')/2]d\tau + g(\sqrt{x_0' + iy_0'}dw_1 - \sqrt{x_0' - iy_0'}dw_1^+)/(i\sqrt{2}),$$

$$dx_2' = [-x_2' + 2\mu_2 \cos(\varphi_2) + (x_0'x_1' + y_0'y_1')/2]d\tau + g(\sqrt{x_0' + iy_0'}dw_2 + \sqrt{x_0' - iy_0'}dw_2^+)/\sqrt{2},$$

$$dy_2' = [-y_2' + 2\mu_2 \sin(\varphi_2) + (y_0'x_1' - x_0'y_1')/2]d\tau + g(\sqrt{x_0' + iy_0'}dw_2 - \sqrt{x_0' - iy_0'}dw_2^+)/(i\sqrt{2}), \tag{10}$$

with

$$\mu_0 = E_0\chi/\gamma\gamma_0, \quad \mu_1 = E_1\chi/\gamma\sqrt{2\gamma_0\gamma}, \quad \mu_2 = E_2\chi/\gamma\sqrt{2\gamma_0\gamma}, \quad dw_1 = \sqrt{2\gamma}dW_1, \quad dw_1^+ = \sqrt{2\gamma}dW_1{}^+,$$
$$dw_2 = \sqrt{2\gamma}dW_2, \quad dw_2^+ = \sqrt{2\gamma}dW_2^+, \quad \mu_0 = \sqrt{P_p/P_{\rm th}}, \quad \mu_1 = \sqrt{\omega_p P_s/(2\omega_s P_{\rm th})}, \quad \mu_2 = \sqrt{\omega_p P_i/(2\omega_i P_{\rm th})}, \tag{11}$$

where P_p, P_s, P_i, and $P_{\rm th}$ are the external power of the pump, injected signal, injected idler, and the threshold, respectively. It is noted that $\mu_0 = 1$ represents the threshold for oscillation when no seed beam is injected into the optical cavity.

III. STEADY-STATE MEAN-VALUE SOLUTION

By taking $dx'(y')_j/d\tau = 0$ $(j = 0 - 2)$ and neglecting the noise terms, the steady-state mean value of Eq. (10) is related to the classical nonlinear equations of motion for the interacting fields,

$$0 = -\gamma_r[x_{0s}' - 2\mu_0 + (x_{1s}'x_{2s}' - y_{1s}'y_{2s}')], \quad 0 = -\gamma_r[y_{0s}' + (x_{1s}'y_{2s}' + x_{2s}'y_{1s}')],$$
$$0 = [-x_{1s}' + 2\mu_1 \cos(\varphi_1) + (x_{0s}'x_{2s}' + y_{0s}'y_{2s}')/2], \quad 0 = [-y_{1s}' + 2\mu_1 \sin(\varphi_1) + (y_{0s}'x_{2s}' - x_{0s}'y_{2s}')/2], \tag{12}$$
$$0 = [-x_{2s}' + 2\mu_2 \cos(\varphi_2) + (x_{0s}'x_{1s}' + y_{0s}'y_{1s}')/2], \quad 0 = [-y_{2s}' + 2\mu_2 \sin(\varphi_2) + (y_{0s}'x_{1s}' - x_{0s}'y_{1s}')/2],$$

where $x'(y')_{js}$ represents the steady-state quadratures.

The stationary solutions of Eq. (12) can be used to examine the classical properties of the system. Because of the difficulty involved in solving the equations analytically, numerical simulation is employed here. From the above equations, we can obtain the intracavity modes,

$$\alpha_j = (x_{js}' + iy_{js}')/2g \quad (j = 1,2), \quad \alpha_0 = (x_{0s}' + iy_{0s}')/(2g\sqrt{2\gamma_r}), \tag{13}$$

and their relative phases,

$$\theta_j = \arg\ \alpha_j = \arg[(x_{js}' + iy_{js}')/(2g)](j = 1,2), \quad \theta_0 = \arg\ \alpha_0 = \arg[(x_{0s}' + iy_{0s}')/(2g\sqrt{2\gamma_r})]. \tag{14}$$

Assuming the seed fields are injected through the output coupler with intensity transmittivity of T $(T \ll 1)$, we can obtain the output fields from the input-output relations,

$$\beta_j = \sqrt{2\gamma}\alpha_j - (1/\sqrt{2\gamma})\varepsilon_j \quad (j = 1,2), \tag{15}$$

where $2\gamma\tau_0 = T$ and τ_0 is the cavity round-trip time. Here it has been assumed that the loss of seed fields is only due to the output-coupling mirror. The output field intensity normalized to the input field can be given by

$$|\beta_j|^2/|\varepsilon_l/\sqrt{2\gamma}|^2 = 4|\alpha_j|^2/\mu_l^2 + \mu_j^2/\mu_l^2 - {\rm Re}[2\alpha_j e^{-i\varphi_j}/\mu_l], \quad j,l \in \{1,2\}. \tag{16}$$

Figure 1 shows the steady-state signal and idler output field intensity normalized to the input signal intensity as a function of the relative phase $\varphi = \varphi_1 + \varphi_2$ between the pump and the injection seed. The amplitudes of the pump and injection signal are fixed, whereas the amplitude of the injection idler varies. If the idler field is absent, both down-converted fields are amplified, and the output intensity remains constant, which means the NOPO is essentially phase insensitive. When the idler injection is present, a phase-sensitive phenomenon will occur, and the output field intensity depends on the relative phase φ and oscillates periodically. If the amplitude of the injection idler and the injection signal is equal and the output signal and idler intensity exhibit the same behavior, one observes the familiar phenomenon of parametric amplification at $\varphi = 2k\pi$ and parametric deamplification at $\varphi = (2k + 1)\pi$.

IV. LINEAR STOCHASTIC EQUATIONS FOR QUANTUM FLUCTUATIONS

To derive the linear stochastic equations, we distinguish two different ways of injecting the seed.

(I) Assuming the seed field is injected through one of the high-reflectivity cavity mirrors, the input-output relation is given by

$$\beta_j = \sqrt{2\gamma}\alpha_j, \quad \theta_j = \arg\ \alpha_j = \arg\ \beta_j, \quad j = 1,2. \tag{17}$$

(II) Assuming the seed field is injected through the output coupler, in this case, the input-output relation is given by

$$\beta_j = \sqrt{2\gamma}\alpha_j - (1/\sqrt{2\gamma})\varepsilon_j, \quad j = 1,2, \quad \phi_j = \arg\ \beta_j, \tag{18}$$

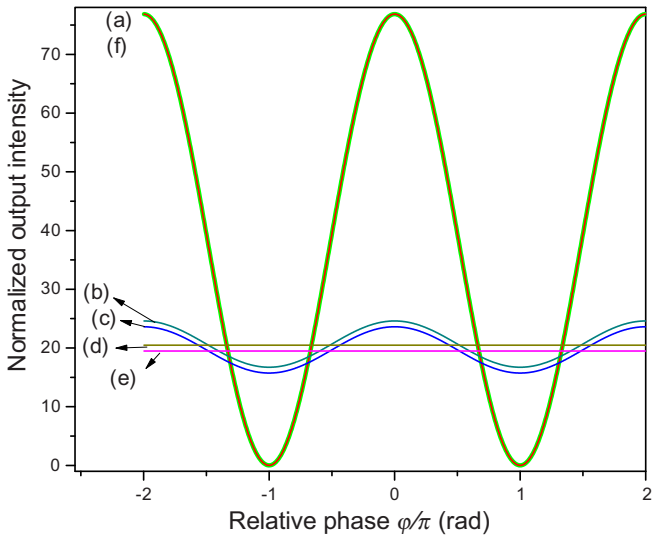

FIG. 1. Steady-state signal and idler output field intensity normalized to the input signal intensity as a function of the relative phase between the pump and the injection seed $\varphi = \varphi_1 + \varphi_2$. For all curves, $\mu_0 = 0.8, \mu_1 = 0.01$. Signal: (a) $\mu_2 = 0.01$; (b) $\mu_2 = 0.001$; (d) $\mu_2 = 0$. Idler: (f) $\mu_2 = 0.01$; (c) $\mu_2 = 0.001$; (e) $\mu_2 = 0$.

For the first case of injecting the seed, the phase of the output field is identical to the intracavity field. Whereas for the second case of injecting the seed, the phase of the output field differs from that of the intracavity field. Such a discrepancy will lead to different external correlation spectra between the signal and the idler fields as we shown in Sec. V.

In order to unify the expressions, we use θ_j to represent the phase for both cases considered above: $\theta_j = \theta_j$ for case I and $\theta_j = \phi_j$ for case II. By using the relative phase θ_j, we define the new field quadratures,

$$\begin{aligned} &X_j = (e^{-i\theta_j}\alpha_j + e^{i\theta_j}\alpha_j^+), \quad Y_j = (e^{-i\theta_j}\alpha_j - e^{i\theta_j}\alpha_j^+)/i, \\ &x_0 = g\sqrt{2\gamma_r}X_0, \quad y_0 = g\sqrt{2\gamma_r}Y_0, \\ &x_1 = gX_1, \quad y_1 = gY_1, \quad x_2 = gX_2, \quad y_2 = gY_2, \end{aligned} \tag{19}$$

where $X_j(x_j)$ is the amplitude quadrature and $Y_j(y_j)$ is the phase quadrature.

The stochastic equations for the new scaled quadratures defined by Eq. (19) can be given by

$$\begin{aligned} dx_0 &= -\gamma_r[x_0 - 2\mu_0\cos(\theta_0) + (x_1x_2 - y_1y_2)\cos(\theta) - (x_1y_2 + x_2y_1)\sin(\theta)]d\tau, \\ dy_0 &= -\gamma_r[y_0 + 2\mu_0\sin(\theta_0) + (x_1y_2 + x_2y_1)\cos(\theta) + (x_1x_2 - y_1y_2)\sin(\theta)]d\tau, \\ dx_1 &= [-x_1 + 2\mu_1\cos(\varphi_1 - \theta_1) + (x_0x_2 + y_0y_2)\cos(\theta)/2 + (y_0x_2 - x_0y_2)\sin(\theta)/2)]d\tau \\ &\quad + g[e^{-i\theta_1}\sqrt{e^{i\theta_0}(x_0 + iy_0)}dw_1 + e^{i\theta_1}\sqrt{e^{-i\theta_0}(x_0 - iy_0)}dw_1^+]/\sqrt{2}, \\ dy_1 &= [-y_1 + 2\mu_1\sin(\varphi_1 - \theta_1) + (y_0x_2 - x_0y_2)\cos(\theta)/2 - (x_0x_2 + y_0y_2)\sin(\theta)/(2)]d\tau \\ &\quad + g[e^{-i\theta_1}\sqrt{e^{i\theta_0}(x_0 + iy_0)}dw_1 - e^{i\theta_1}\sqrt{e^{-i\theta_0}(x_0 - iy_0)}dw_1^+]/(i\sqrt{2}), \\ dx_2 &= [-x_2 + 2\mu_2\cos(\varphi_2 - \theta_2) + (x_0x_1 + y_0y_1)\cos(\theta)/2 + (y_0x_1 - x_0y_1)\sin(\theta)/2]d\tau \\ &\quad + g[e^{-i\theta_2}\sqrt{e^{i\theta_0}(x_0 + iy_0)}dw_2 + e^{i\theta_2}\sqrt{e^{-i\theta_0}(x_0 - iy_0)}dw_2^+]/\sqrt{2}, \\ dy_2 &= [-y_2 + 2\mu_2\sin(\varphi_2 - \theta_2) + (y_0x_1 - x_0y_1)\cos(\theta)/2 - (x_0x_1 + y_0y_1)\sin(\theta)/2]d\tau \\ &\quad + g[e^{-i\theta_2}\sqrt{e^{i\theta_0}(x_0 + iy_0)}dw_2 - e^{i\theta_2}\sqrt{e^{-i\theta_0}(x_0 - iy_0)}dw_2^+]/(i\sqrt{2}), \end{aligned} \tag{20}$$

where $\theta = \theta_1 + \theta_2 - \theta_0$. To investigate the quantum properties of the system, we can introduce a formal perturbation expansion in powers of the parameter g,

$$x_k = \sum_{n=0}^{\infty} g^n x_k^{(n)}, \quad y_k = \sum_{n=0}^{\infty} g^n y_k^{(n)}, \tag{21}$$

The zeroth term of the above expansion represents the property of the classical field of order $1/g$, whereas the first-order term corresponds to quantum fluctuations of order 1. The nonlinear corrections coming from higher-order terms correspond to the quantum fluctuations of order g and higher, which can be neglected when the NOPO is below and not very close to the threshold [24]. This region is just what concerns us in the present paper. Using Eq. (21), the first-order set of equations can be written as

$$\begin{aligned} dx_0^{(1)} &= -\gamma_r\left[x_0^{(1)} + \left(x_{1s}x_2^{(1)} + x_{2s}x_1^{(1)} - y_{1s}y_2^{(1)} - y_{2s}y_1^{(1)}\right)\cos(\theta) - \left(x_{1s}y_2^{(1)} + x_1^{(1)}y_{2s} + x_{2s}y_1^{(1)} + x_2^{(1)}y_{1s}\right)\sin(\theta)\right]d\tau, \\ dy_0^{(1)} &= -\gamma_r\left[y_0^{(1)} + \left(x_{1s}y_2^{(1)} + x_1^{(1)}y_{2s} + x_{2s}y_1^{(1)} + x_2^{(1)}y_{1s}\right)\cos(\theta) + \left(x_{1s}x_2^{(1)} + x_{2s}x_1^{(1)} - y_{1s}y_2^{(1)} - y_{2s}y_1^{(1)}\right)\sin(\theta)\right]d\tau, \\ dx_1^{(1)} &= \left[-x_1^{(1)} + \left(x_{0s}x_2^{(1)} + x_{2s}x_0^{(1)} + y_{0s}y_2^{(1)} + y_{2s}y_0^{(1)}\right)\cos(\theta)/2 + \left(-x_{0s}y_2^{(1)} - x_0^{(1)}y_{2s} + x_{2s}y_0^{(1)} + x_2^{(1)}y_{0s}\right)\sin(\theta)/2\right]d\tau \\ &\quad + \left[e^{-i\theta_1}\sqrt{e^{i\theta_0}(x_{0s} + iy_{0s})}dw_1 + e^{i\theta_1}\sqrt{e^{-i\theta_0}(x_{0s} - iy_{0s})}dw_1^+\right]/\sqrt{2}, \\ dy_1^{(1)} &= \left[-y_1^{(1)} + \left(-x_{0s}y_2^{(1)} - x_0^{(1)}y_{2s} + x_{2s}y_0^{(1)} + x_2^{(1)}y_{0s}\right)\cos(\theta)/2 - \left(x_{0s}x_2^{(1)} + x_{2s}x_0^{(1)} + y_{0s}y_2^{(1)} + y_{2s}y_0^{(1)}\right)\sin(\theta)/2\right]d\tau \\ &\quad + \left[e^{-i\theta_1}\sqrt{e^{i\theta_0}(x_{0s} + iy_{0s})}dw_1 - e^{i\theta_1}\sqrt{e^{-i\theta_0}(x_{0s} - iy_{0s})}dw_1{}^+\right]/\sqrt{2}i, \end{aligned}$$

$$
\begin{aligned}
dx_2^{(1)} =& \big[-x_2^{(1)} + \big(x_{0s}x_1^{(1)} + x_{1s}x_0^{(1)} + y_{0s}y_1^{(1)} + y_{1s}y_0^{(1)}\big)\cos(\theta)/2 + \big(-x_{0s}y_1^{(1)} - x_0^{(1)}y_{1s} + x_{1s}y_0^{(1)} + x_1^{(1)}y_{0s}\big)\sin(\theta)/2\big]d\tau \\
&+ \big[e^{-i\theta_2}\sqrt{e^{i\theta_0}(x_{0s} + i\,y_{0s})}dw_2 + e^{i\theta_2}\sqrt{e^{-i\theta_0}(x_{0s} - i\,y_{0s})}dw_2^{+}\big]/\sqrt{2}, \\
dy_2^{(1)} =& \big[-y_2^{(1)} + \big(-x_{0s}y_1^{(1)} - x_0^{(1)}y_{1s} + x_{1s}y_0^{(1)} + x_1^{(1)}y_{0s}\big)\cos(\theta)/2 - \big(x_{0s}x_1^{(1)} + x_{1s}x_0^{(1)} + y_{0s}y_1^{(1)} + y_{1s}y_0^{(1)}\big)\sin(\theta)/2\big]d\tau \\
&+ \big[e^{-i\theta_2}\sqrt{e^{i\theta_0}(x_{0s} + i\,y_{0s})}dw_2 - e^{i\theta_2}\sqrt{e^{-i\theta_0}(x_{0s} - i\,y_{0s})}dw_2^{+}\big]/\sqrt{2}i.
\end{aligned} \tag{22}
$$

Equations (22) are linear stochastic equations with nonclassical Gaussian white noise. It is useful to introduce combined field quadratures including both the signal and the idler modes, and the two-mode quadratures are defined as

$$
x_{\pm} = \big(x_1^{(1)} \pm x_2^{(1)}\big)/\sqrt{2}, \quad y_{\pm} = \big(y_1{}^{(1)} \pm y_2{}^{(1)}\big)/\sqrt{2}. \tag{23}
$$

Taking the steady-state solutions for the pumped field quadratures, the linear quantum fluctuations in the combined field quadratures can be written as

$$
\begin{aligned}
dx_+ &= \{-Ax_+ + Ex_- + Fy_+ + Gy_-\}d\tau + dn_{x+}, \quad dx_- = \{-Bx_- + Ex_+ - Fy_- - Gy_+\}d\tau + dn_{x-}, \\
dy_+ &= \{-Cy_+ + Ey_- + Fx_+ - Gx_-\}d\tau + dn_{y+}, \quad dy_- = \{-Dy_- + Ey_+ - Fx_- + Gx_+\}d\tau + dn_{y-},
\end{aligned} \tag{24}
$$

where the coefficients of the equations are defined as

$$
\begin{aligned}
A &= 1 - [x_{0s}\cos(\theta)/2 + y_{0s}\sin(\theta)/2] + (x_{1s} + x_{2s})^2/4 + (y_{1s} + y_{2s})^2/4, \\
B &= 1 + [x_{0s}\cos(\theta)/2 + y_{0s}\sin(\theta)/2] + (x_{1s} - x_{2s})^2/4 + (y_{1s} - y_{2s})^2/4, \\
C &= 1 + [x_{0s}\cos(\theta)/2 + y_{0s}\sin(\theta)/2] + (x_{1s} + x_{2s})^2/4 + (y_{1s} + y_{2s})^2/4, \\
D &= 1 - [x_{0s}\cos(\theta)/2 + y_{0s}\sin(\theta)/2] + (x_{1s} - x_{2s})^2/4 + (y_{1s} - y_{2s})^2/4, \\
E &= \big(x_{1s}^2 - x_{2s}^2\big)/4 + \big(y_{1s}^2 - y_{2s}^2\big)/4, \\
F &= y_{0s}\cos(\theta)/2 - x_{0s}\sin(\theta)/2, \quad G = y_{2s}x_{1s}/2 - x_{2s}y_{1s}/2,
\end{aligned} \tag{25}
$$

and the noise terms are defined as

$$
dn_{x+} = \big(dn_{x_1} + dn_{x_2}\big)/\sqrt{2}, \quad dn_{x-} = \big(dn_{x_1} - dn_{x_2}\big)/\sqrt{2}, \quad dn_{y+} = \big(dn_{y_1} + dn_{y_2}\big)/\sqrt{2}, \quad dn_{y-} = \big(dn_{y_1} - dn_{y_2}\big)/\sqrt{2}, \tag{26}
$$

where

$$
\begin{aligned}
dn_{x_1} &= \sqrt[4]{x_{0s}^2 + y_{0s}^2}[dw_{x1}\cos(\theta_1) - i\,dw_{y1}\sin(\theta_1)], \quad dn_{x_2} = \sqrt[4]{x_{0s}^2 + y_{0s}^2}[dw_{x2}\cos(\theta_2) - i\,dw_{y2}\sin(\theta_2)], \\
dn_{y_1} &= -i\sqrt[4]{x_{0s}^2 + y_{0s}^2}[-i\,dw_{x1}\sin(\theta_1) + dw_{y1}\cos(\theta_1)], \quad dn_{y_2} = -i\sqrt[4]{x_{0s}^2 + y_{0s}^2}[-i\,dw_{x2}\sin(\theta_2) + dw_{y2}\cos(\theta_2)].
\end{aligned} \tag{27}
$$

The new Wiener increments in Eq. (27) are expressed by

$$
dw_{x1(y1)}(t) = [dw_1(\tau) \pm dw_1^{+}(\tau)]/\sqrt{2}, \quad dw_{x2(y2)}(\tau) = [dw_2(\tau) \pm dw_2^{+}(\tau)]/\sqrt{2}, \tag{28}
$$

and satisfy the following correlation relations,

$$
\langle dw_{x1}dw_{x2}\rangle = d\tau, \quad \langle dw_{y1}dw_{y2}\rangle = d\tau, \tag{29}
$$

with all other correlations vanishing. Equation (24) can be used to predict quantum correlation and squeezing in the combined quadratures, which correspond to the squeezed and antisqueezed combined quadratures obtained in the linearized theory.

V. OUTPUT NOISE SPECTRA AND ENTANGLEMENT

To make a comparison between the theoretical predictions with the experiment, the quantum noise spectra outside the cavity should be calculated. We will therefore proceed by transforming to frequency space via Fourier transform of the combined field quadratures,

$$
f(\Omega) = (1/\sqrt{2\pi})\int_{-\infty}^{+\infty} d\tau\; e^{-i\Omega\tau} f(\tau), \tag{30}
$$

and the white-noise terms,

$$
\xi_{x,y}(\Omega) = (1/\sqrt{2\pi})\int_{-\infty}^{+\infty} d\tau\; e^{-i\Omega\tau}\xi_{x,y}(\tau), \tag{31}
$$

with the correlation,

$$
\langle\xi_a(\Omega)\rangle = 0, \quad \langle\xi_{a1}(\Omega)\xi_{b2}(\Omega')\rangle = \delta_{ab}\delta(\Omega + \Omega'). \tag{32}
$$

The first-order stochastic equations in the frequency domain can be written as

$$
\begin{aligned}
i\Omega\tilde{x}_+(\Omega) &= \{-A\tilde{x}_+(\Omega) + E\tilde{x}_-(\Omega) + F\tilde{y}_+(\Omega) + G\tilde{y}_-(\Omega)\} \\
&\quad + d\tilde{n}(\Omega)_{x+}, \\
i\Omega\tilde{x}_-(\Omega) &= \{-B\tilde{x}_-(\Omega) + E\tilde{x}_+(\Omega) - F\tilde{y}_-(\Omega) - G\tilde{y}_+(\Omega)\} \\
&\quad + d\tilde{n}(\Omega)_{x-}, \\
i\Omega\tilde{y}_+(\Omega) &= \{-C\tilde{y}_+(\Omega) + E\tilde{y}_-(\Omega) + F\tilde{x}_+(\Omega) - G\tilde{x}_-(\Omega)\} \\
&\quad + d\tilde{n}(\Omega)_{y+},
\end{aligned}
$$

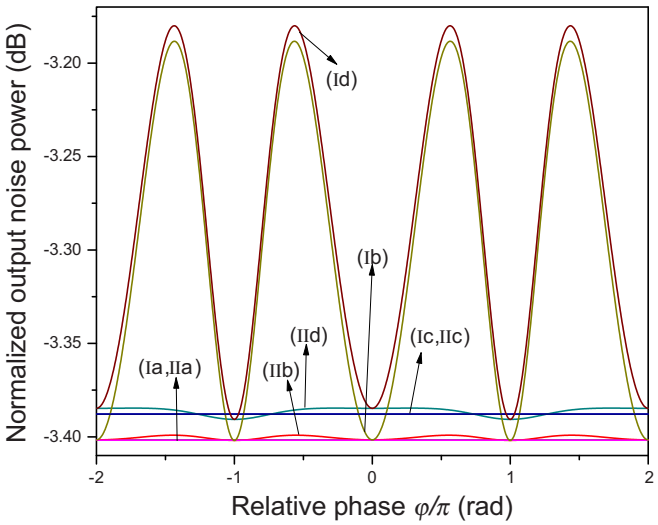

FIG. 2. Normalized output noise power V_{x_-} and V_{y_+} as a function of the relative phase between the pump and the injection seed with $\mu_0 = 0.8, \mu_1 = 0.01$, and $\Omega = 0$. (Ia) and (IIa): $V_{x_-}, \mu_2 = 0$; (Ib) and (IIb): $V_{x_-}, \mu_2 = 0.001$; (Ic) and (IIc): $V_{y_+}, \mu_2 = 0$; (Id) and (IId): V_{y_+}, $\mu_2 = 0.001$. I and II denote the two different ways of injecting the seed.

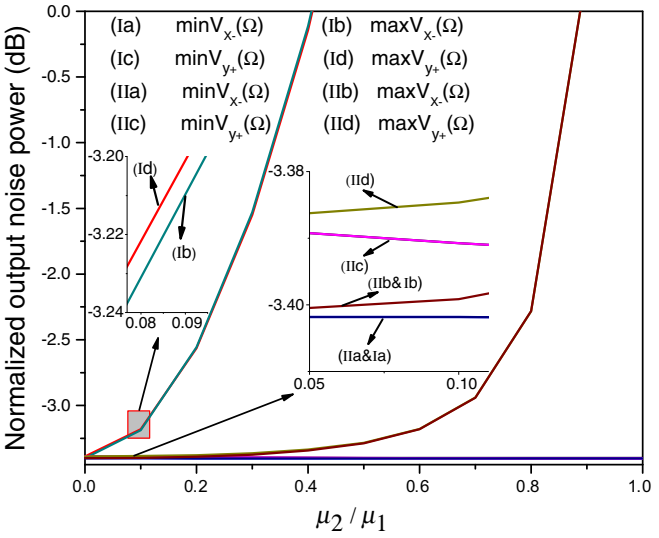

FIG. 3. The minimum and maximum values of V_{x_-} and V_{y+} versus the injection ratio μ_2/μ_1 with $\mu_0 = 0.8$ and $\Omega = 0$.

$$
\begin{aligned}
i\Omega\tilde{y}_-(\Omega) &= \{-D\tilde{y}_-(\Omega) + E\tilde{y}_+(\Omega) - F\tilde{x}_-(\Omega) + G\tilde{x}_+(\Omega)\} \\
&\quad + d\tilde{n}(\Omega)_{y-}, \qquad (33)
\end{aligned}
$$

where

$$
\begin{aligned}
d\tilde{n}(\Omega)_{x\pm} &= \left[d\tilde{n}_{x_1}(\Omega) \pm d\tilde{n}_{x_2}(\Omega)\right]/\sqrt{2}, \\
d\tilde{n}(\Omega)_{y\pm} &= \left[d\tilde{n}_{y_1}(\Omega) \pm d\tilde{n}_{y_2}(\Omega)\right]/\sqrt{2}, \\
d\tilde{n}_{x_1}(\Omega) &= \sqrt[4]{x_{0s}^2 + y_{0s}^2}[\xi_{x1}(\Omega)\cos(\theta_1) - i\xi_{y1}(\Omega)\sin(\theta_1)], \\
d\tilde{n}_{x_2}(\Omega) &= \sqrt[4]{x_{0s}^2 + y_{0s}^2}[\xi_{x2}(\Omega)\cos(\theta_2) - i\xi_{y2}(\Omega)\sin(\theta_2)], \\
d\tilde{n}_{y_1}(\Omega) &= -i\sqrt[4]{x_{0s}^2+y_{0s}^2}[-i\xi_{x1}(\Omega)\sin(\theta_1)+\xi_{y1}(\Omega)\cos(\theta_1)], \\
d\tilde{n}_{y_2}(\Omega) &= -i\sqrt[4]{x_{0s}^2+y_{0s}^2}[-i\xi_{x2}(\Omega)\sin(\theta_2)+\xi_{y2}(\Omega)\cos(\theta_2)]. \qquad (34)
\end{aligned}
$$

From Eq. (33) we can obtain the analytical solutions of $\tilde{x}_+(\Omega)$, $\tilde{x}_-(\Omega)$, $\tilde{y}_+(\Omega)$, and $\tilde{y}_-(\Omega)$. The correlation spectrum of the internal (intracavity) combined field quadratures $\langle\tilde{y}_+(\Omega)\tilde{y}_+(\Omega')\rangle$ and $\langle\tilde{x}_-(\Omega)\tilde{x}_-(\Omega')\rangle$ are then calculated straightforwardly. The external correlation spectrum is obtained in the positive-P representation by the relation,

$$
\begin{aligned}
V_{ij}^{\text{out}}(\Omega)\delta(\Omega+\Omega') &= \delta_{ij} + 2\sqrt{\gamma_i^{\text{out}}\gamma_j^{\text{out}}}\langle\Delta X_i(\Omega)\Delta X_j(\Omega')\rangle_P, \\
&\quad \{i,j = y_+, x_-\}, \qquad (35)
\end{aligned}
$$

where $\langle\Delta X_i(\Omega)\Delta X_j(\Omega')\rangle_P$ is the internal correlation spectrum and γ^{out} denotes the cavity mode damping rate due to the output coupler. To fit our experimental results in Sec. VI, we choose $\gamma^{\text{out}}/\gamma = 0.55$ in the following theoretical analysis.

Figure 2 shows the output noise power of the combined field quadratures at $\Omega = 0$. If only the signal field is injected, the properties of the quantum correlation are the same for both cases of injecting the seed, and the quadrature correlations V_{x_-} and V_{y_+} of the output signal and idler fields remain untouched regardless of the change in the relative phase. When both the signal and the idler fields are injected, the correlation spectra start to oscillate periodically versus the relative phase. For the relative phase of $\varphi = \pi$, the injection of the idler can lead to a little improvement in V_{y_+}. It is noted that the degree of the amplitude quadrature correlation is higher than that of the phase quadrature anticorrelation if the injection field has a nonzero mean value and they tend to be equal when $\mu_2/\mu_0, \mu_1/\mu_0 \to 0$. For the injection field of $\mu_1 = 0.01$ and $\mu_2 = 0.001$, the quantum correlations in case I show much better stability than that in case II when the relative phase varies.

Figure 3 shows the minimum and maximum values of V_{x_-} and V_{y+} at different injection ratios μ_2/μ_1. For each injection ratio, the relative phase is used as the free parameter to find the desired extreme values. It is evident that optimal squeezing of V_{x_-} and V_{y+} remain almost unchanged at any ratio of the injected seed. In case I, the worst squeezing of V_{x_-} and V_{y+} degrades with the injection ratio quickly, and the squeezing vanishes at $\mu_2/\mu_1 \sim 0.4$. Around 3 dB squeezing can be generated if the injection ratio is limited to $\mu_2/\mu_1 < 0.13$. In case II, the worst squeezing can exist in a broad range of the ISR and gradually vanishes at $\mu_2/\mu_1 \sim 0.9$. Note that even if the relative phase is free running, over 3 dB of squeezing can still be obtained given the injection ratio is limited to $\mu_2/\mu_1 < 0.7$. The observed phenomena denote that if the seed is injected from the output coupler, the NOPO will allow for robust generation of two-mode quantum entanglement even if the relative phase is free running and the ISR is high.

Given the correlation spectrum of the combined quadratures, the quantum entanglement can be evaluated readily based on the inseparability criterion proposed by Duan *et al.* [25]. The entanglement is guaranteed provided that the correlation spectra of the combined quadratures satisfy $V_{x_-}(\Omega) + V_{y_+}(\Omega) < 2$.

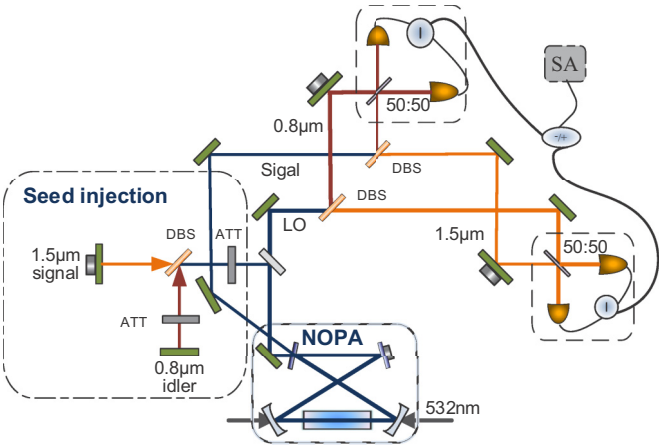

FIG. 4. Schematic of the experimental setup. Dichroic beam splitter (DBS) and optical attenuator (ATT).

VI. EXPERIMENT

In order to verify the robustness of the NOPO when the seed is injected through the output coupler, we design an experiment shown in Fig. 4. The NOPO with a bow tie configuration is pumped by a 532-nm laser from two opposite directions [20] with a pump power of 1.2 times the threshold in one direction and 0.6 times the threshold in the opposite direction. The main portion of the 0.8- and 1.5-μm bright down-conversion beams act as the local oscillator for homodyne detection, and a small portion of them serves as the seed beam which is injected through the output coupler of the NOPO below threshold. To facilitate the fine control of the injection ratio μ_2/μ_1, a dichroic beam splitter is employed to separate the signal and idler, and the intensity of the idler is then adjusted by using a variable optical attenuator. It is noted that when no seed is injected, there are still very weak signal and idler fields that can be measured at the output of the NOPO below threshold. Such residual down-conversion fields are probably due to the backscattering light of the nonlinear crystal and cavity mirror, etc.

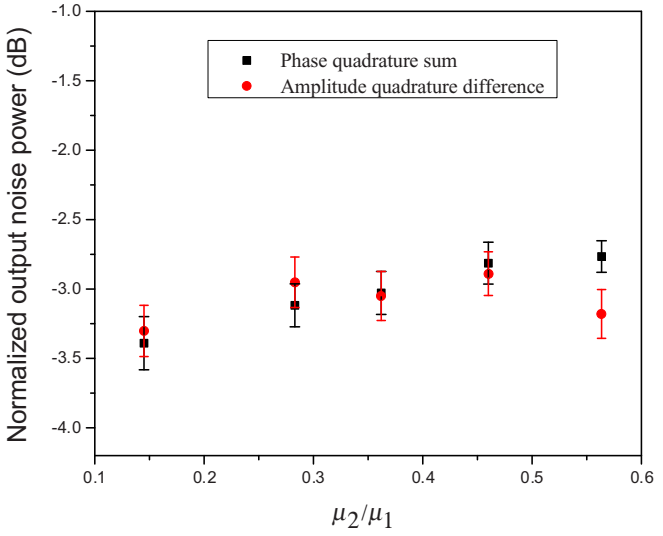

FIG. 5. Measured amplitude quadrature difference and phase quadrature sum noise power versus the different injection ratios $\mu_2/\mu_1 = 0.15, 0.28, 0.36, 0.46, 0.56$. The relative phase between the seed and the pump is scanned from 0 to 2π during the measurement.

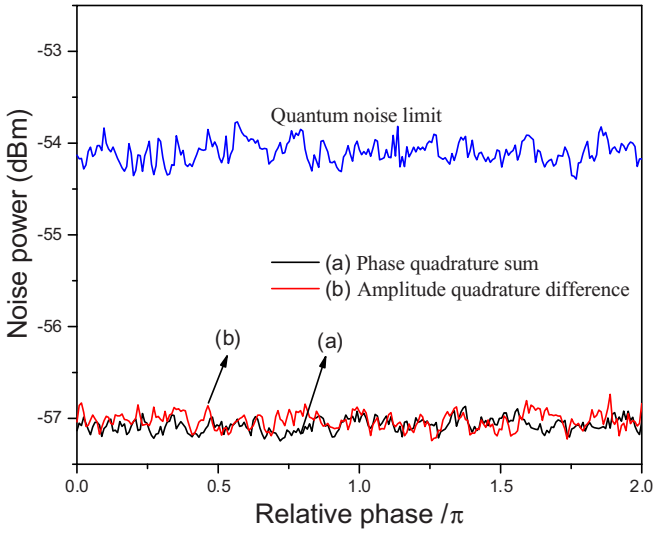

FIG. 6. Amplitude quadrature difference and phase quadrature sum noise power for injection ratio $\mu_2/\mu_1 = 0.36$. The relative phase between the seed and the pump is scanned from 0 to 2π. Analysis frequency: 3 MHz.

Figure 5 shows the measured amplitude quadrature difference and phase quadrature sum noise power versus the different injection ratios μ_2/μ_1 at an analysis frequency of 3 MHz. The electronic dark noises of the homodyne detectors that are around 20 dB below the quantum noise limit are not subtracted. During the measurement, the relative phase between the pump and the seed is scanned linearly from 0 to 2π, and the error bars denote the corresponding fluctuations of the observed quadrature correlation. It can be seen from Fig. 5 that $\sim$3 dB of entanglement can be generated at the injection ratio of $\mu_2/\mu_1 = 0.56$ even if the relative phase undergoes a 2π phase change. Figure 6 displays the noise power of the amplitude quadrature difference and the phase quadrature sum as a function of the scanned relative phase between the seed and the pump at $\mu_2/\mu_1 = 0.36$. The quadrature correlations V_{x_-} and V_{y_+} of the output signal and idler fields remain almost unchanged regardless of the scanning of the relative phase. The experimental results are inconsistent with the theoretical analysis.

VII. CONCLUSIONS

To summarize, we have analyzed in detail the effect of the injected idler-to-signal ratio on the classical and quantum behaviors of the output fields from a NOPO. Our analysis shows that the injection of the idler field will inevitably convert the NOPO from the phase-insensitive region when only the signal field is injected into the phase-sensitive region where both the classical mean-field and the quantum correlation spectra of the combined quadratures vary with the relative phase between the pump and the seed. There exists a specific

relative phase (0°) where the entanglement can persist across a whole range of the injection idler-to-signal ratio and the degradation of the entanglement is trivial. It is found that if the seed is injected from the output coupler instead of the high-reflectivity cavity mirror, a high degree of two-mode quantum entanglement can still be yielded regardless of the relative phase even if the injection idler-to-signal ratio is as high as $\mu_2/\mu_1 \sim 0.7$. Such a phenomenon is also verified in experiment. The results we presented can provide useful guidance for the preparation of two-color continuous variable quantum entanglement from a NOPO with an injected seed.

ACKNOWLEDGMENTS

This research was supported by the National Natural Science Foundation of China (NSFC) (Grants No. 61378010 and No. 11504219), the Natural Science Foundation of Shanxi Province (Grant No. 2014011007-1), and the Program for the Outstanding Innovative Teams of Higher Learning Institutions of Shanxi.

[1] T. C. Ralph and P. K. Lam, Nat. Photonics **3**, 671 (2009).
[2] E. Knill, R. Laflamme, and G. Milburn, Nature (London) **409**, 46 (2000).
[3] V. Giovannetti, S. Lloyd, and L. Maccone, Nat. Photonics **5**, 222 (2011).
[4] L. S. Madsen, V. C. Usenko, M. Lassen, R. Filip, and U. L. Andersen, Nat. Commun. **3**, 1083 (2012).
[5] P. Walther, K. J. Resch, T. Rudolph, E. Schenck, H. Weinfurter, V. Vedral, M. Aspelmeyer, and A. Zeilinger, Nature (London) **434**, 169 (2005).
[6] P. M. Anisimov, G. M. Raterman, A. Chiruvelli, W. N. Plick, S. D. Huver, H. Lee, and J. P. Dowling, Phys. Rev. Lett. **104**, 103602 (2010).
[7] M. D. Reid and P. D. Drummond, Phys. Rev. A **40**, 4493 (1989).
[8] P. D. Drummond and M. D. Reid, Phys. Rev. A **41**, 3930 (1990).
[9] Z. Y. Ou, S. F. Pereira, H. J. Kimble, and K. C. Peng, Phys. Rev. Lett. **68**, 3663 (1992).
[10] Y. Zhang, H. Wang, X. Y. Li, J. T. Jing, C. D. Xie, and K. C. Peng, Phys. Rev. A **62**, 023813 (2000).
[11] C. Schori, J. L. Sorensen, and E. S. Polzik, Phys. Rev. A **66**, 033802 (2002).
[12] A. S. Villar, L. S. Cruz, K. N. Cassemiro, M. Martinelli, and P. Nussenzveig, Phys. Rev. Lett. **95**, 243603 (2005).
[13] J. Jing, S. Feng, R. Bloomer, and O. Pfister, Phys. Rev. A **74**, 041804 (2006).
[14] X. L. Su, A. H. Tan, X. J. Jia, Q. Pan, C. D. Xie, and K. C. Peng, Opt. Lett. **31**, 1133 (2006).
[15] N. B. Grosse, S. Assad, M. Mehmet, R. Schnabel, T. Symul, and P. K. Lam, Phys. Rev. Lett. **100**, 243601 (2008).
[16] A. S. Coelho, F. A. S. Barbosa, K. N. Cassemiro, A. S. Villar, M. Martinelli, and P. Nussenzveig, Science **326**, 823 (2009).
[17] X. M. Guo, C. D. Xie, and Y. M. Li, Phys. Rev. A **84**, 020301(R) (2011).
[18] X. J. Jia, Z. H. Yan, Z. Y. Duan, X. L. Su, H. Wang, C. D. Xie, and K. C. Peng, Phys. Rev. Lett. **109**, 253604 (2012).
[19] O. Pinel, P. Jian, R. M. de Araújo, J. X. Feng, B. Chalopin, C. Fabre, and N. Treps, Phys. Rev. Lett. **108**, 083601 (2012).
[20] X. M. Guo, J. J. Zhao, and Y. M. Li, Appl. Phys. Lett. **100**, 091112 (2012).
[21] S. Yokoyama, R. Ukai, S. C. Armstrong, C. Sornphiphatphong, T. Kaji, S. Suzuki, J. Yoshikawa, H. Yonezawa, N. C. Menicucci, and A. Furusawa, Nat. Photonics **7**, 982 (2013).
[22] B. Coutinho dos Santos, K. Dechoum, A. Z. Khoury, L. F. da Silva, and M. K. Olsen, Phys. Rev. A **72**, 033820 (2005).
[23] A. S. Lane, M. D. Reid, and D. F. Walls, Phys. Rev. A **38**, 788 (1988).
[24] K. Dechoum, P. D. Drummond, S. Chaturvedi, and M. D. Reid, Phys. Rev. A **70**, 053807 (2004).
[25] L. M. Duan, G. Giedke, J. I. Cirac, and P. Zoller, Phys. Rev. Lett. **84**, 2722 (2000).